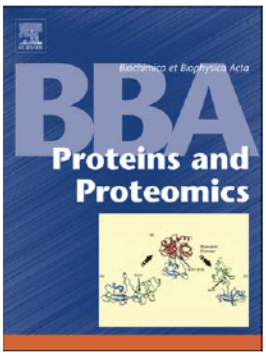

On the Ca^{2+} binding and conformational change in EF-hand domains: Experimental evidence of Ca^{2+}-saturated intermediates of N-domain of calmodulin

Abdessamad Ababou, Mariola Zaleska, Mark Pfuhl

PII: S1570-9639(17)30045-6
DOI: doi:10.1016/j.bbapap.2017.03.003
Reference: BBAPAP 39909

To appear in: *BBA - Proteins and Proteomics*

Received date: 15 October 2016
Revised date: 7 March 2017
Accepted date: 9 March 2017

Please cite this article as: Abdessamad Ababou, Mariola Zaleska, Mark Pfuhl, On the Ca^{2+} binding and conformational change in EF-hand domains: Experimental evidence of Ca^{2+}-saturated intermediates of N-domain of calmodulin, *BBA - Proteins and Proteomics* (2017), doi:10.1016/j.bbapap.2017.03.003

On the Ca^{2+} binding and conformational change in EF-hand domains: Experimental evidence of Ca^{2+}-saturated intermediates of N-domain of calmodulin

Abdessamad Ababou [a,b] *, Mariola Zaleska [c], Mark Pfuhl [d]

[a] *Department of Pathology, University of Cambridge, Tennis Court Road, Cambridge CB2 1QP, UK*

[b] *University of East London, School of Health, Sport and Bioscience, Water Lane, London E15 4LZ, UK*

[c] *Department of Biochemistry, University of Cambridge, Tennis Court Road, Cambridge,CB2 1QP, UK*

[d] *Cardiovascular and Randall Division, King's College London, London, SE1 1UL, United Kingdom*

* Corresponding author: *email: a.ababou10@yahoo.co.uk. Tel: +44* 02082234589.

Abstract

Double mutation of Q41L and K75I in the N-domain of calmodulin (N-Cam) stabilizes the closed form of N-Cam such that binding of Ca^{2+} in solution no longer triggers a conformational change to the open form, and its Ca^{2+} binding affinity decreases dramatically. To further investigate the solvation effects on the structure, Ca^{2+} binding affinity and conformational dynamics of this N-Cam double mutant in the Ca^{2+} saturated state, we solved its X-ray structure. Surprisingly, the structure revealed an open conformation of the domain which contradicts its closed conformation in solution. Here we provide evidence that crystallization conditions were responsible for this Ca^{2+}-saturated domain open conformation in the crystal. Importantly, we demonstrate that the presence of the crystallization co-precipitant and alcohols were able to induce a progressive opening of the closed form of this domain, in Ca^{2+} saturated state, in solution. However, in the Ca^{2+} depleted state, addition of alcohols was unable to induce any opening of this domain in solution. In addition, in the Ca^{2+} saturated state, the molecular dynamics simulations show that while N-Cam can populate the open and closed conformation, the N-Cam double mutant exclusively populates the closed conformation. Our results provide experimental evidence of intermediate conformations of Ca^{2+}-saturated N-Cam in solution. We propose that conformational change of Ca^{2+} sensor EF-hand domains depends on solvation energetics, Ca^{2+} binding to promote the full open form, Ca^{2+} depleted state conformational dynamics, and the chemical properties of the molecules nearby key residues such as those at positions 41 and 75 in N-Cam.

Keywords: EF-hand domain, Ca^{2+} binding, conformational change, solvation enegetics, X-ray crystallography, MD simulation.

1. Introduction

Calcium binding EF-hand proteins form a large family and their common structural and functional unit is an EF-hand domain [1, 2] consisting of a pair of EF-hand motifs [3, 4]. Ca^{2+} sensor EF-hand domains change conformation upon Ca^{2+} binding, from a closed to an open form, such as calmodulin EF-hand domains, N-domain (N-Cam) and C-domain (C-Cam), while Ca^{2+} buffer or modulator EF-hand domains, such as calbindin D9k (Clb), exhibit only subtle structural changes [5]. However, there is a large diversity in the structural response of EF-hand domains to Ca^{2+} binding, as well as in their Ca^{2+} affinity [4, 6-18]. Such diverse structural and biochemical properties of these domains support the idea of their direct involvement in the broad range of cellular functions achieved by EF-hand proteins [19-24].

To date, much of the structural, functional and biochemical properties of many of EF-hand domains have been extensively investigated and well established concepts, such as the coupling between Ca^{2+} binding, conformational change and protein target interactions, are widely accepted [4-6, 12-15, 17, 18, 25-34]. To contribute to enhancing our understanding of these domains' crucial link between conformational change and Ca^{2+} binding, we have provided evidence that in solution mutation of two key polar residues at positions 41 and 75, Gln41 and Lys75, in N-Cam by their corresponding nonpolar residues Leu and Ile from Clb resulted in the stabilization of the closed form of N-Cam such that the hydrophobic variant Q41L-K75I (QLKI) no longer changes its conformation to the open form upon Ca^{2+} binding, and its Ca^{2+} binding affinity dramatically decreases [35]. Subsequently, we have shown that long range effectors, such as the introduction of the L39F mutation, can play an important role in the differences of Ca^{2+} binding affinities between these EF-hand domains, without affecting their conformational change in the presence of Ca^{2+} [36]. Furthermore, we have demonstrated that conformational dynamics of EF-hand domains can differentiate them in terms of Ca^{2+} binding affinity and extent of conformational change, which are directly involved in their functional purpose [37]. However, despite our utmost effort in understanding the structural and biochemical characteristics and properties of EF-hand domains, the experimental evidence for the conformational change mechanism and the

variations of Ca^{2+} binding affinities within the EF-hand domains family, even though their Ca^{2+} loops exhibit highly conserved coordinating residues, are yet to be fully provided.

Consequently, to understand the effect of mutations Q41L and K75I on the Ca^{2+}-saturated structure and Ca^{2+} binding affinity of N-Cam at the atomic level, we have solved the X-ray structure of Ca^{2+}-saturated QLKI (QLKI+Ca^{2+}) and investigated its conformational dynamics in solution using molecular dynamics (MD) simulation. Surprisingly, the structure of QLKI+Ca^{2+} revealed an open conformation that contradicts our solution findings and the MD simulation showed that the structure of QLKI+Ca^{2+}, during the trajectory, adopts a close conformation as expected in solution. In this work, we demonstrate that the crystallization conditions were responsible for the structural opening of QLKI+Ca^{2+}. In solution, and only in the presence of Ca^{2+}, polar organic molecules such as alcohols induce the structural opening of QLKI+Ca^{2+}. Furthermore, we discuss our findings in terms of the mechanism of conformational change and the Ca^{2+} binding affinity of Ca^{2+} sensor EF-hand domains. We suggest that the molecular composition of the local environment, around and at the corresponding positions 41 and 75, is important for the conformational change in these domains, which mimics the early stages of their protein target binding, and the Ca^{2+} affinity change most probably correlates with conformational dynamics of the Ca^{2+} depleted state as previously reported [37].

2. Materials and Methods

2.1. Protein preparation and purification

The N-terminal domain of the recombinant human calmodulin, residues 1-78, N-CamY (F19Y and D78Y) and its hydrophobic variant Q41L-K75I (QLKI) were subcloned from a plasmid containing full length human calmodulin using standard cloning techniques, as previously reported [35]. All the proteins were expressed and purified as previously reported; except for the second purification step where we used size-exclusion chromatography [35, 37]. The concentrations of the proteins were determined in 6M GdmCl using absorbance spectroscopy and a molar extinction coefficient of Tyr at 280 nm of 1420 M^{-1} cm^{-1}.

2.2. Chemicals

The alcohols, Ethanol and Isopropanol, buffers, GdmCl and PEG 400 were purchased from Sigma. All the standard laboratory chemicals were of the highest grade commercially available.

2.3. Circular Dichroism spectroscopy

Circular Dichroism (CD) spectra were collected on an Aviv Model SF202 CD spectrophotometer equipped with a Hamilton microlab 500 series titrator. Near-UV CD spectra were collected between 310 to 250 nm with an averaging time at each wavelength of 3 s. After each increase in the alcohol or PEG 400 concentration, the sample was allowed to equilibrate for 2.5 min. All CD measurements were corrected by subtracting the buffer spectra. The stock solutions were prepared fresh daily. All experiments were carried out in 20 mM MOPS, pH 7.2, 100 mM KCl. For Ca^{2+} free and saturated measurements, 0.1 mM EDTA and 1 mM $CaCl_2$ were used, respectively. The CD data collection was repeated 3-5 times.

2.4. Crystallization of QLKI+Ca^{2+}

QLKI+Ca^{2+} Crystals were grown by the hanging drop vapour diffusion method at 15 ^{o}C, using a protein stock concentration of ~20 mg/ml. The drops were made by mixing 2.0 μl of QLKI in 20 mM MOPS, pH 7.2, 100 mM KCl, 1 mM $CaCl_2$, with 2.0 μl of the well solution containing 0.1 M HEPES buffer at pH 7.5, 0.25 M $CaCl_2$, 37% (v/v) PEG 400, and equilibrated against 1 ml of the well solution. The crystals were grown in 3-5 days and were cryoprotected by stepwise addition of cryoprotectant as the well solution plus 20% glycerol or 25% ethylene glycol, before being flash-frozen in liquid nitrogen.

2.5. X-ray diffraction collection, structure phasing and refinement

X-ray diffraction data were collected at 100 K on the beamline ID29 at the European Synchrotron Radiation Facility (ESRF, Grenoble, France). X-ray data sets were indexed and integrated using iMosflm [38] and scaled using Scala or Aimless in the CCP4 suite [39]. The structures were solved by molecular replacement using Phaser [40] or Molrep

[41]. The structure was solved using PDB entry 1CLL truncated to residue 78 which corresponds to the length of QLKI used in this work. The structure refinement was performed in two steps: First we used the recently reported refinement strategy combining the Rosetta sampling methodology and energy function with reciprocal-space X-ray refinement in Phenix [42], and then we continue the refinement using Phenix [43]. The structure was completed with iterative rounds of manual model-building with Coot [44] and refinement in Phenix. Figures were prepared using PyMol (www.pymol.org).

2.6. Molecular Dynamics Simulation and Trajectory Analysis

We have used the Ca^{2+}-saturated N-Cam domain structure from Ca^{2+}-saturated calmodulin structure, PDB entry 1CLL, and we have changed Phe19 to Tyr and Asp78 to Tyr using AMBER14 [45]. We have used our Ca^{2+}-saturated QLKI structure after removing the PEG 400 and water molecules, and used the PDB entry 4ICB for the Ca^{2+}-saturated structure of Clb. Similarly, we have used the apo form of the N-Cam domain structure from calmodulin (PDB code 1CFD), and built QLKI using Q41L and K75I mutations in N-Cam domain structure. Then the proteins were energy minimized using AMBER14. The MD simulations were performed, at constant temperature and pressure, on fully immersed proteins in a rectangular water box withTIP3P water. The water box was built using a cutoff of 8 Å between the solute and the box edge. The AMBER force field parm99 was used for the protein [46] and TIP3P parameters for the water [47]. The time step was 1.5 fs with bonds fixed by SHAKE [48]. The formal charge of N-CamY, QLKI and Clb were -6, –7 and –3 e, respectively, and the protein system neutralization was achieved by adding Na^{+} ions. The temperature was 300 K, van der Waals interactions were truncated at 10.0 Å, while electrostatic interactions were fully calculated with the Particle Mesh Ewald method [49]. For each protein system a 50 ps trajectory for solvent equilibration was calculated, and following the equilibration a trajectory of 100 ns was calculated. Same MD simulation protocol was used for our QLKI+Ca^{2+} structure including the partial PEG 400 molecule, which we completed by reflecting the absence of any close interaction with QLKI+Ca^{2+}, as the complex between QLKI+Ca^{2+} and PEG400. However, for the ligand we have calculated its atomic charges using ANTECHAMBER [50] and used GAFF force field [51].

Structural properties of the proteins were analyzed as function of time using the root-mean-square deviation from the starting structure (RMSD), the root-mean-square fluctuation from the starting structure (RMSF), and solvent-accessible surface area (SASA), using AMBER14 and VMD [52]. Principal component analysis (PCA) was performed and since the first three eigenvectors account for almost the total motions, we have projected our MD trajectories into the three-dimensional subspace defined by the top three principal components (PC1, PC2, and PC3). The interhelical angles were calculated using interhlx (Kyoko Yap, University of Toronto) and the helices were defined as H1 (E7,S17), H2 (L32, S38), H3 (A46, E54), and H4 (F65, R74). The chosen angles are those that vary the most between the closed and open form of the domain (Angles between helices (deg) in N-Cam - closed/open (PDB entry: 1CFD/1CLL): H1-H2: 137/88, H1-H3: -90/-160, H3-H4: 133/87).

2.7. Accession numbers

The atomic coordinates and structure factors of Ca^{2+}-saturated QLKI have been deposited at Protein Data Bank with the accession code 5DSU.

3. Results

3.1 Crystal structure of Ca^{2+}-saturated QLKI

Taking into account that QLKI+Ca^{2+} adopts a closed conformational state in solution, as we previously reported [35], first we have tried to solve the crystal structure of QLKI+Ca^{2+} using the Ca^{2+} free N-Cam (PDB entry 1CFD), however, we were unsuccessful. Subsequently, we used the Ca^{2+}-saturated N-Cam (N-Cam+Ca^{2+}) (PDB entry 1CLL), and surprisingly we were able to solve our QLKI+Ca^{2+} structure. The data collection and refinement statistics are shown in **Table 1**. Comparison of QLKI+Ca^{2+} structure with the N-Cam+Ca^{2+} from the reported structure of Ca^{2+}-saturated calmodulin [53] shows clearly that QLKI+Ca^{2+} is in the open form with an RMSD of 1.14 Å (**Fig. 1A**). Both Ca^{2+} loops, I and II, and the majority of hydrophobic residues in the domain core, as well as in the Ca^{2+} loops, are nearly identical to those of N-Cam+Ca^{2+} (**Fig. 1B, 1C**). However, there are some dissimilarities consisting of few side chains, such as I75 pointing toward the inside of QLKI+Ca^{2+} while K75 clearly pointing toward the outside of

N-Cam+Ca^{2+} (**Fig. 1C**), residues at the N-terminus, and importantly the inter-helical angles between helices H1-H2 and H2-H4, where substantial differences occurred and in particular for H2-H4 (**Table 2**). QLKI+Ca^{2+} exhibits a slightly closed form than in N-Cam+Ca^{2+}, which could be linked to the mutations Q41L in H2 and K75I in H4 (**Fig. 1C**). Indeed, within EF-hand domains, the angles between the four helices (H1, H2, H3, and H4) are important for the analysis of their conformational changes [6].

To understand why the crystal structure of QLKI+Ca^{2+} is open, we inspect closely its crystal packing in $P3_221$ space group. The structure shows the presence of a large crystal contact with another QLKI+Ca^{2+} molecule where both molecules face each other with their hydrophobic surface which is well known to interact with protein targets of calmodulin (**Fig. S1**). Interestingly, this crystal contact exhibits resemblance to the conformation of Ca2+-saturated calmodulin in complex with a protein target in wrap-around binding mode [26]. Hence, we compared our crystal contact structure to those of Ca^{2+}-saturated calmodulin, in complex with small molecules, in space group $P3_221$, since our protein samples and crystallization conditions were free from any targets of calmodulin (PDB entries: 1A29, 1CTR, 1LIN, 1QIV and 3IF7). While our QLKI+Ca^{2+} structure superimposes well with the N-domains of these structures, their C-domain did not match well the crystal contact in our QLKI+Ca^{2+} structure, since the latter was largely off in both translation and rotation (see example in **Fig. S2**).

Nevertheless, this crystal contact in such orientation has the potential to shift the equilibrium of QLKI+Ca^{2+} from closed to open, as the domain may have less solvation penalty to offset from exposing such hydrophobic surface to the solvent.

3.2. Crystal versus solution structure of Ca^{2+}-saturated QLKI

The unexpected open form of the crystal structure of QLKI+Ca^{2+}, prompted us to investigate further the reasons that may lead to such outcome beyond crystal packing. Consequently, we have probed the effect of crystallization conditions on the conformational state of QLKI+Ca^{2+} using near-UV CD spectroscopy. Strikingly, exchanging our standard QLKI+Ca^{2+} buffer (20 mM MOPS, pH 7.2, 100 mM KCl, 1 mM $CaCl_2$) with the crystallization solution (0.1 M HEPES buffer at pH 7.5, 0.25 M $CaCl_2$, 37% (v/v) PEG 400) resulted in a CD spectrum which indicates that our QLKI+Ca^{2+}

structure is now open in solution (**Fig. 2**). This clearly shows that one or several components of the crystallization buffer may be responsible for the opening of this domain in the crystal structure, and hence ruling out the involvement of the crystal packing in such structural opening of QLKI+Ca^{2+}.

Since our crystallization condition contained 250 mM Ca^{2+} we have recorded the CD spectra of QLKI+Ca^{2+} and N-CamY+Ca^{2+} in their standard buffer in the presence of 300 mM Ca^{2+}. However, no substantial changes occurred as QLKI+Ca^{2+} kept its structure in the closed form, which clearly ruled out the excess of Ca^{2+} to play any role in the opening of QLKI+Ca^{2+} in solution (**Fig. 2B**). Interestingly, when we recorded the spectra in the presence of 37% PEG 400, there was clear spectrum change of QLKI+Ca^{2+}, similar to the one in **Fig. 2A**, revealing its open from in solution (data not shown). Furthermore, we observe a remarkable and consistent change in the CD spectra of QLKI+Ca^{2+} in the presence of different amounts of PEG 400, which increases with the increase of PEG 400, as represented at 277 nm (**Fig. 2C**). In contrast, no change was observed for N-CamY+Ca^{2+}, as it is already in an open form (**Fig. 2C**).

Close inspection of the hydrophobic patch in the structure of QLKI+Ca^{2+} shows the presence of an incomplete PEG 400 molecule, with only 3 repeats of [O-CH_2-CH_2] instead of 8-9 in the complete molecule, with well assigned electron density as it was initially found within the unbiased difference electron density map prior to its placement (**Fig. 3**). This partial PEG 400 molecule is surrounded by residues from helices H1, H2 and H4, as shown in **Fig. 3D** within a sphere with a radius, atom to atom, of 4 Å. The presence of this PEG 400 in our QLKI+Ca^{2+} structure provides a rational to the effect of PEG 400 on the opening of QLKI+Ca^{2+} in solution as we report here (**Fig. 2C**). Since PEG 400 has two hydroxyl groups (-OH), at the start and the end of the molecule, we hypothesized that (1) if PEG 400 induces the opening of QLKI+Ca^{2+} in solution then possibly alcohol molecules may have a similar effect on QLKI+Ca^{2+}, and (2) the aliphatic chain size may also play a role in the opening of QLKI+Ca^{2+} in solution, as it should make better hydrophobic contact with the hydrophobic surface patch of QLKI+Ca^{2+}. To verify our hypotheses, we used ethanol and isopropanol to probe the effect of the alcohol group and the increase of the alcohol aliphatic chain, respectively (**Fig. 4A**). Near-UV CD spectra of QLKI+Ca^{2+} collected with increasing amount of alcohol for up to ~ 33% and represented at 277 nm, show consistent increase of the CD signal (**Fig. 4B**),

while an overall small to no change in CD signal was observed for N-CamY+Ca^{2+} (**Fig. 4C**). Importantly, isopropanol exhibits larger effect on the opening of QLKI+Ca^{2+} in solution than ethanol, and apparently this holds also for N-CamY+Ca^{2+}, at least at lower percentages of alcohols (**Fig. 4C**). However, for N-CamY+Ca^{2+} this may simply reflect the conformational dynamics change of the domains [54, 55]. It may also suggest that the presence of alcohols, in particular Isopropanol, reveals the true complete open conformation of N-CamY+Ca^{2+}, similar to the open conformation in the presence of its protein targets. This result clearly suggests that the key molecular features directly involved in the opening of QLKI+Ca^{2+} in solution are the alcohol group and the aliphatic chain size of the alcohol molecule. Note that such properties constitute the foundation of all protein targets binding sites of calmodulin, which are dominated by the IQ motifs [24, 34, 56, 57].

Subsequently, we have addressed the question about the effect of alcohol molecules on the opening of the closed state of Ca^{2+} depleted QLKI and N-CamY. The near-UV CD spectra of N-CamY and QLKI in the presence of ethanol and isopropanol revealed no major change which demonstrates that these EF-hand domains maintain their closed form (**Fig. S3**). This result provides evidence that in the absence of Ca^{2+} neither alcohol group nor the aliphatic chain size were able to shift the closed form of the apo QLKI and N-CamY toward their open forms.

3.3. Conformational dynamics investigations of Ca^{2+}-saturated N-CamY, QLKI and Clb

We have performed MD simulations of QLKI+Ca^{2+} and N-CamY+Ca^{2+} to assess the effect of the double mutation on the conformational dynamics of N-CamY in the presence of Ca^{2+}. We also performed MD simulation of Clb+Ca^{2+} as a control, since Clb maintains its closed conformation in the presence of Ca^{2+}. To assess the sampling of conformational space achieved during our MD simulations we performed principal component analysis (PCA) for these EF-hand domains. The 2D plot of each domain conformation, as projected into PC1, PC2 and PC3 modes, shows a good conformational sampling amount by the proteins (**Fig. 5A, Fig. S4**); however, it is noticeable that conformational sampling of N-CamY+Ca^{2+} is largely wider as compared to QLKI+Ca^{2+} and Clb+Ca^{2+}(**Fig. 5A, Fig. S4**). To assess the stability and any global structural changes of the proteins we have plotted their backbone RMSD as function of

time (**Fig. 5B**). While the RMSD plot for Clb+Ca^{2+} shows an overall highly stable protein with minimum structural variations during the whole MD trajectory, N-CamY+Ca^{2+} and QLKI+Ca^{2+} present several structural variations with the largest change occurring in the time range of 60-100 ns for N-CamY+Ca^{2+}. In contrast, QLKI+Ca^{2+}'s RMSD changes were irregular at the start and overall stable between 55 ns to 100 ns.

Interestingly, Clb+Ca^{2+} presents the lowest backbone atoms fluctuations and has almost similar trend as QLKI+Ca^{2+}, with the only substantial difference at residues 57-62 (**Fig. 5C**). However, while N-CamY+Ca^{2+} and QLKI+Ca^{2+} have three similar regions (called (1), (2) and (3) in **Fig. 5C**) with noticeable higher backbone fluctuations, N-CamY+Ca^{2+} shows, by far larger fluctuations in those regions, which are located in helix-1 (H1), helix-2 (H2), helix-3 (H3), the linker between H2 and H3, and part of the second Ca2+ loop (**Fig. 5D**). Note that in N-CamY+Ca^{2+} the largest fluctuations between H2 and H3 for the exact region (2) have been reported with similar observation [58]. Importantly, even though the overall crystal structure of QLKI+Ca^{2+} may resemble the well known open structure of N-CamY+Ca^{2+}, our backbone fluctuations results show that the flexibility of QLKI+Ca^{2+} is substantially low in comparison with N-CamY+Ca^{2+}.

To further investigate the conformational dynamics behavior of our EF-hand domains in the presence of Ca^{2+}, we have calculated the distance between the key residues at positions 41 and 75 in N-CamY+Ca^{2+} and QLKI+Ca^{2+}, and the corresponding positions 39 and 73 in Clb+Ca^{2+}, and the solvent accessible surface area (SASA) of particular highly buried residues L32 and F68 in N-CamY+Ca^{2+} and QLKI+Ca^{2+}, and residues L28 and F66 in Clb+Ca^{2+}. Overall the distance between L39 and I73 in Clb+Ca^{2+} was unchanged during the MD trajectory with a value of ~ 8.5 Å (**Fig. 6A**), while the distance between L41 and I75 in QLKI+Ca^{2+} changed substantially from ~ 15.0 Å to ~ 8.5 Å during the MD trajectory with the major change taking place in the first 10 ns, as shown in **Fig. S5**. Interestingly, although the starting distance between Q41 and K75 in N-CamY+Ca^{2+} was close to the distance in QLKI+Ca^{2+}, a sharp increase of this distance occurred during the first 20 ns reaching high values of ~ 28 Å, followed by several fluctuations between large values of ~ 20 Å and smaller values of ~ 8.2 Å, which was reached around ~ 52 ns (**Fig. 6A**). However, beyond that time this distance increased for the rest of the trajectory reaching its starting value ~ 15.0 Å. The SASA analysis of the chosen buried residues reveals that, with exception of L32 in QLKI+Ca^{2+} at the start of

the trajectory (0 - 3ns), these residues are highly protected from the solvent in QLKI+Ca^{2+} and Clb+Ca^{2+} (**Fig. 6B, 6C**). In contrast, in N-CamY+Ca^{2+} these residues were accessible to the solvent to a different extent at the start, around the middle and by the end of the MD trajectory (**Fig. 6B, 6C**). Furthermore, the SASA analysis of the positions 41 and 75 in N-CamY+Ca^{2+} and their corresponding positions 39 and 73 in Clb+Ca^{2+} revealed an overall similar trend as observed for the above highly buried residues (**Fig. 6B, 6C**). In fact, while the SASA of Q41 and K75 in N-CamY+Ca^{2+} changed dramatically, the SASA of these and corresponding residues in QLKI+Ca^{2+} and Clb+Ca^{2+} shows fewer changes and rather stable average values, when excluding the start of the trajectory for QLKI+Ca^{2+} (**Fig. S6**).

To check for possible conformational changes in our EF-hand domains, we have calculated their interhelical angles along the MD trajectories, and focused on the angles that change substantially between the closed and open form of N-Cam, as reported in **Fig. 6D-F**. Close inspection of the plots shows clearly that N-CamY+Ca^{2+} exhibits substantial and frequent changes in its interhelical angles, in particular at the start, around the middle and the end of the MD trajectory. Indeed, the angle values at the start of the trajectory revealed N-CamY+Ca^{2+} to be populating a conformational state that is further open, followed by a more closed conformational state reaching a peak around 60-70 ns, but then beyond this time period there was a return to the open conformation (**Fig. 6D-F**). In contrast, Clb+Ca^{2+} presents no substantial changes of these angles during the MD trajectory, which confirms its well known closed conformation in either solution or in crystal forms [59, 60]. However, while these angles in QLKI+Ca^{2+} were nearly matching those of an open conformation at the start of the trajectory, soon after changes took place for all these angles leading to values reflecting a change in this domain conformation towards a close conformation (**Fig. 6D-F**).

Our MD trajectory analysis of these EF-hand domains (**Fig. 5, 6**), clearly points to the presence of structural changes with the hallmark of an EF-hand domain conformational change between closed and open forms. Consequently, we have analyzed snapshot structures taken from the MD trajectory of these domains. **Fig. S7** depicts the overlay of these domains' structures at 0 ns, 50 ns, and 100 ns, along with the closed form of N-Cam in absence of Ca^{2+} when appropriate. Interestingly, the overlay of structures of N-CamY+Ca^{2+} at 0 and 50 ns shows a high RMSD of 4.2 Å, while superposition of the

structure at 50 ns with the N-Cam structure in the closed form (PDB entry 1CFD) gives a value of 2.4 Å. Clearly N-CamY+Ca^{2+} structure shifts from an open to a closed form despite the presence of Ca^{2+}. However, by the end of the MD trajectory the overlay of the structures at 0 ns and 100 ns presents a lower RMSD of 2.1 Å, which becomes 6.8 Å for the overlay of this structure with N-Cam. This reveals that N-CamY+Ca^{2+} structure has returned to its starting open form structure. In contrast, the overlay of structures of QLKI+Ca^{2+} at 0 ns, 50 ns, 100 ns shows that this domain was shifting from the initial open form to the closed form as judged by their respective RMSD of 4.3 Å and 3.9 Å. These values were only 2.6 Å and 2.5 Å when the structure superpositions between 50 ns and 100 ns with N-Cam were performed, respectively, revealing clearly that QLKI+Ca^{2+} is indeed adopting a closed form similar to the structure we have reported in solution for this domain [35]. For Clb+Ca^{2+}, instead, the superimposition of its structures at 0 ns, 50 ns, and 100 ns, reveals no substantial changes and importantly the domain maintained its closed form during the MD trajectory (**Fig. S7**).

4. Discussion

Previously we have shown that in solution QLKI+Ca^{2+} adopts a closed form and its Ca^{2+} binding affinity decreased significantly [35]. To understand how solvation energetics affect the conformational change of QLKI+Ca^{2+} and why the Ca^{2+} binding affinity for this EF-hand domain decreased, we have solved the crystal structure of QLKI+Ca^{2+}. Surprisingly, this crystal structure revealed an open form structure of this EF-hand domain, which totally contradicts our solution findings. Our detailed investigation of QLKI+Ca^{2+} structure and the cause behind this discrepancy revealed that the crystallization conditions were responsible for the opening of QLKI+Ca^{2+} structure, and thus rules out the crystal packing explanation as previously suggested for N-Cam+Ca^{2+} [58]. Indeed, we have shown that addition of the precipitant PEG 400 to the closed form of QLKI+Ca^{2+} in solution resulted in this domain changing from a closed conformation to an open conformation (**Fig. 2**). Furthermore, we have shown that addition of alcohols such Ethanol and Isopropanol to QLKI+Ca^{2+} in solution produced similar results, namely the shift of QLKI+Ca^{2+} structure from a closed to an open conformation (**Fig. 4**). However, the size of the alcohol's aliphatic chain plays an important role in the extent the opening of QLKI+Ca^{2+}. Indeed, Isopropyl induces larger changes in the near-UV CD signal when compared to Ethanol (**Fig. 4B**). This suggests that the effect of the alcohol

aliphatic chain size on the extent of the opening of QLKI+Ca^{2+} structure in solution may correlate with the importance of the number of hydrophobic residues in protein targets of calmodulin [24, 61, 62]. Note that a complete opening of QLKI+Ca^{2+} is reached gradually with an increasing amount of either PEG 400 or alcohols, which suggest that these molecules probably bind, non specifically, the exposed hydrophobic surface of this EF-hand domain during its conformational change (**Fig. 2** and **4**).

To check on the binding specificity of PEG400 to QLKI+Ca^{2+}, in solution, we have performed MD simulation of QLKI+Ca^{2+} in complex with PEG400 using our X-ray structure. The MD simulation data show that PEG400 molecule moved spontaneously from its original binding site to other part of the exposed hydrophobic surface of QLKI+Ca^{2+}, with the possibility of complete dissociation of the complex during longer MD trajectory (**Fig. 7D** and **Fig. S8**). This demonstrates that PEG400 binding to QLKI+Ca^{2+} is non-specific. Interestingly, while after 40 ns in the MD trajectory the distance between L45 and I75 and the interhelical angle between helices H3 and H4 were maintained at closed conformation values (**Fig. 7A, 7C** and **7E**), the interhelical angle values between helices H1 and H2 reflected rather those of an open conformation (**Fig. 7B** and **Fig. S9**). The movement of PEG400 during the MD trajectory clearly affects the conformational state of QLKI+Ca^{2+}, which is in line with our experimental data (**Fig. 2** and **4**).

This clearly shows that although the solvation effect was crucial in conformational shift of QLKI+Ca^{2+} toward the closed form in solution [35], a change in the molecular composition of the local environment nearby positions 41 and 75 can easily reverse that conformational shift from closed to open form. Our MD simulation of QLKI+Ca^{2+} strongly supports this view, since this EF-hand domain changed its conformation from open, at the start of the trajectory, to a closed during and until the end of the trajectory (**Fig. 5, 6** and **Fig. S7**). In fact, since QLKI+Ca^{2+} is submerged in a box of water then the resulting behavior of this domain is similar to the one we observe experimentally in solution (**Fig. 2A**, QLKI+Ca^{2+}(Buffer)). Importantly, the induced conformational change of QLKI+Ca^{2+} in solution, by either PEG 400 or alcohols, highlights the experimental observation of intermediate conformations of N-Cam similar to those that are taking place during its interactions with its protein targets in the presence of Ca^{2+}.

Nevertheless, beyond the change in the local environment's molecular composition at positions 41 and 75, Ca^{2+} binding is an important step prior to any conformational change to take place; otherwise in the absence of Ca^{2+} the addition of alcohols has no effect on the conformational state of either N-CamY or QLKI (**Fig. S3**). While this clearly holds for N-Cam, as shown here, we anticipate that this may not hold for C-Cam because of the energetics differences between the Ca^{2+} free N-Cam and C-Cam, which mainly consists of the highly dynamic nature of C-Cam when compared to N-Cam (see further details in [37]). Indeed, this is largely supported by the binding of C-Cam to several protein targets in the absence of Ca^{2+}, while N-Cam does not [56, 63-65].

Interestingly, the extent of the opening of QLKI+Ca^{2+} is slightly lower in comparison with N-CamY+Ca^{2+} (**Fig. 2** and **4**). This is an important observation, since errors in protein concentration were ruled out because we used highly purified proteins, we estimate the protein concentration based on Tyr's absorption, our experiments were highly reproducible, and we have repeated our experiments several times. To estimate this extent of the opening of QLKI+Ca^{2+} as compared to N-CamY+Ca^{2+} we used a simple equation relating both near-UV CD signals of the fully closed QLKI+Ca^{2+} and fully open N-CamY+Ca^{2+} in solution, as follows:

$$\Theta = \alpha\,\Theta(\text{N-CamY+Ca}^{2+}) + (1-\alpha)\,\Theta(\text{QLKI+Ca}^{2+})$$

where Θ is the ellipticity signal and α is the open form fraction. Our crude and modest fit of the CD signal of QLKI+Ca^{2+} in the presence of crystallization buffer, shows that on average the extent of the opening of this domain is about 75% (between 70% and 80%) of the opening of N-CamY+Ca^{2+} (**Fig. S10**). Such difference reflects the balance between solvation effect and the molecular composition at the local environment of positions 41 and 75, capable of initiating and inducing the conformational change of QLKI+Ca^{2+}. In fact, the hydrophobic nature of these residues, L41 and I75, tends to bring them as close as possible, which in turn affects the opening of the domain as reflected by the change in the packing of the aromatic residues in the core of the domain leading to a decrease in the near-UV CD signal. Although, this may not be clearly observed in the crystal structure of QLKI+Ca^{2+}, with the exception of the small changes in the side chain of F9 and F62, the large change in the interhelical angle between H2 and H4, and the proximity between L41 and I75 may be reflected in the observed CD

signal (**Fig. 1** and **Table 2**). Significantly, these data show that our QLKI+Ca^{2+} variant in solution reports on the intermediate conformational states of N-CamY+Ca^{2+} that occur transiently prior to its full open form. Indeed, addition of alcohol molecules progressively shifted QLKI+Ca^{2+} from a closed to an open form, and thus providing an exceptional opportunity to have experimental evidence on the existence of these elusive intermediate states of N-CamY+Ca^{2+}, as well as in general for Ca^{2+} sensor EF-hand domains. In fact, others have made attempts to capture these intermediate conformational states in Ca^{2+} sensor EF-hand domains but only limited success was achieved [66-68].

Our initial aim was to understand, at the atomic level, the solvation effect on the conformational shift of QLKI+Ca^{2+} to the closed form in solution, and on the Ca^{2+} binding affinity of this EF-hand domain. However, while the unexpected open form of the crystal structure of QLKI+Ca^{2+} may seem disappointing at first, it provides us with an excellent opportunity to understand further the intertwined aspects of solvation energetics, conformational change and Ca^{2+} binding in Ca^{2+} sensor EF-hand domains. Indeed, beyond our investigation of the solvation effects in N-Cam using QLKI, our solution data on QLKI+Ca^{2+} actually captured an intermediate conformation of N-CamY+Ca^{2+} in a closed form, which is a transient conformational state that is difficult to observe experimentally in solution, and the progressive opening of the structure of QLKI+Ca^{2+} in solution, in the presence of PEG 400 or alcohols, revealed further intermediate conformational states providing the experimental evidence of the transient intermediate conformations of N-Cam that occur during its interactions with its protein targets in the presence of Ca^{2+}.

The crystallization conditions caused the QLKI+Ca^{2+} structure to adopt an open form as opposed to its closed form in solution, resulting in the typical pentagonal bipyramidal Ca^{2+} coordination geometry with coordinating residues identical to the wild type N-Cam, and prevented us from getting the closed form structure of this domain in the presence of Ca^{2+} (**Fig. 1**). Nevertheless, the structure of Ca^{2+} loaded calmodulin with the N-Cam trapped in closed form, using mutations Q41C and K75C leading to a disulfide bridge formation (called here QCKC+Ca^{2+}), has been reported [69]. In fact, this QCKC+Ca^{2+} structure shows clearly that N-Cam can bind Ca^{2+} in a closed form, and possibly with similar conformation to our QLKI+Ca^{2+} structure in solution. Interestingly, this structure

revealed that both Ca^{2+} ions lack the bidentate coordination by either E31 or E67, the important glutamate residues at position 12 in the Ca^{2+} loops [4]. In principal, at first this seems to explain the low Ca^{2+} binding affinity we reported for our QLKI-Ca^{2+} complex formation [35], since lacking E31 and E67 coordination will undoubtedly weaken the binding of Ca^{2+} ions and change its favored canonical coordination in an EF-hand motif. However, it is very intriguing to note that the introduction of mutation L39F into QLKI (L39F-QLKI), which is far from the Ca^{2+} loops I and II centers by an average distance of ~ 16 Å and ~ 21 Å, respectively, leads to an increase of Ca^{2+} binding affinity of this EF-hand domain (ΔG^{o}_{2Ca} ~ -14.1 kcal/mol), which is slightly higher than N-CamY (ΔG^{o}_{2Ca} ~ -13.9 kcal/mol). Crucially, it resulted in unchanged structural response of this EF-hand domain to the Ca^{2+} binding in solution, namely L39F-QLKI+Ca^{2+} maintained its closed form [36]. The most plausible explanation for such an increase in Ca^{2+} affinity to L39F-QLKI should be attributed to the presence of the bidentate coordination of the Ca^{2+} with E31 and E67, otherwise it is difficult to imagine such increase of Ca^{2+} affinity in the absence of these bidentate coordinating residues. Furthermore, a long-range effect in this case has the hallmark of conformational dynamics change as the most plausible explanation to the origin of L39F effect on the Ca^{2+} binding to L39F-QLKI, as recently we have reported for several electrostatic mutants of N-CamY [37]. Indeed, such conformational dynamics changes may affect substantially the Ca^{2+} loops, and possibly the whole Ca^{2+} depleted domain, leading to the Ca2+ affinity change and the possibility of E31 and E67 to coordinate the Ca^{2+} ions, as previously reported [37].

To check on how the conformational dynamics of the Ca^{2+} depleted state of these EF-hand domains may affect their Ca^{2+} affinity, we have performed MD simulations of N-CamY and QLKI. Whilst the RMSD plots of both domains are overall nearly similar, revealing the stability of the domains with no major structural changes, the distances between Cα's of residues at positions 41 and 75 are substantially different, with an average distance of ~ 9 Å and ~ 17 Å for QLKI and N-CamY, respectively (**Fig. S11A, B**). The change of the interhelical angles during the MD trajectories revealed that while both domains are still in an overall closed form, N-CamY tends to slightly open its conformation and QLKI tends to further close its conformation, as shown in the comparison of their structures at 0 ns and 100 ns (**Fig. S12**). Interestingly, like the observed flexibility at region (2), H2-loop-H3, (**Fig. 5D**), here we observe the slight opening or the closing of these domains to be well highlighted at the same region (**Fig.**

S12B, C). Surprisingly, although QLKI tends to further close its conformation, its Ca^{2+} loops exhibit higher backbone flexibility when compared to those in N-CamY, in particular for Ca^{2+} loop II (**Fig. S11C**). This finding allows us to speculate that the low Ca^{2+} affinity of QLKI may be directly linked to its Ca^{2+} loop flexibility in the absence of Ca^{2+}. Strikingly, looking back at our MD simulations data of the electrostatic variants and in particular the mutant QEKE (Q41E-K75E), which has the highest Ca^{2+} binding affinity (ΔG^{o}_{2Ca} ~ -15.3 kcal/mol) [37], we found that the flexibility of the Ca^{2+} loops of this domain to be lower than those of N-CamY (**Fig. S13**). Note that QEKE exhibited the highest changes of the interhelical angles (toward the open form) and the distance between residues E41 and E75 [37]. Although, further investigations are necessary to understand this correlation between the EF-hand domain opening/**closing** tendency, lower/**higher** flexibility of its Ca^{2+} loops and higher/**lower** Ca^{2+} affinity, it is interesting to notice that, at least, among N-CamY variants, like QEKE and QLKI, such correlation holds. Nevertheless, these observations clearly point to the conformational dynamics of these EF-hand domains as an important factor in their Ca^{2+} affinity differences, as previously reported [37], rather than the direct involvement of their bidentate coordinating residues at position 12 in Ca^{2+} loops, such as E31 and E67 in N-Cam.

To further investigate our hypothesis on the E31 and E67 coordination of Ca^{2+} in either L39F-QLKI+Ca^{2+} or QLKI+Ca^{2+} in solution, we have used the structure of QCKC+Ca^{2+} to model our QLKI-Ca^{2+} in closed form [69]. Interestingly, the energy minimization of QCKC+Ca^{2+} structure resulted in the coordination of Ca^{2+} in Ca^{2+} loop II by E67, whereas in the Ca^{2+} loop I E31 remained unable to coordinate the Ca^{2+} (**Table S1**). Note that such a Ca^{2+} coordination by E67 did not affect the interhelical angles of QCKC+Ca^{2+}, in particular for the helices 1 and 3 that are not involved in C41-C75 disulfide bridge (**Table S2**). We made the mutations C41L-C75I to model our QLKI+Ca^{2+} structure in closed form in solution, and performed further energy minimization of this domain. Close inspection of the latter revealed that the Ca^{2+} ion, in Ca^{2+} loop I, has gained the bidentate coordination as provided by E31 (**Fig. 8** and **Table S1**). This suggests that the removal of the disulfide bridge between C41 and C75 in QCKC+Ca^{2+}, was imperative to get this domain out of a potential energy trap which hindered Ca^{2+} coordination in Ca^{2+} loop I by E31. Surprisingly, even though both Ca^{2+} ions have the bidentate coordination provided by E31 and E65, the interhelical angles and the small β-sheet, between I27 and I63, revealed minor to no change as compared to the energy

minimized structure of QCKC+Ca^{2+} (**Fig. 8** and **Table S2**). The main changes take place in the Ca^{2+} loops, where D22/D24 and D58/N60 undergo substantial movement to maintain the Ca^{2+} coordination. In fact, to better appreciate the movement of the Ca^{2+} loops, we overlay of the structures of QCKC+Ca^{2+}, before the energy minimization, and the energy minimized QLKI+Ca^{2+}, as depicted in **Fig. S14**. This clearly suggests that the bidentate coordinations could not be the main driving force in the conformational change in Ca^{2+} sensor EF-hand domains, which opposes the claims by previous reports [70-73]. Our MD simulations of QLKI+Ca^{2+} strongly support this view since during the MD trajectory the structure of QLKI+Ca^{2+} not only shifts toward the closed form of the domain but crucially maintains the bidentate coordination by the glutamate residues, E31 and E67 at position 12 in Ca^{2+} loops, which were absent in the QCKC+Ca^{2+} crystal structure (**Fig. S7** and **S15**). Further support for this view came from the close inspection of the Ca^{2+} loops of the closed form of N-Cam+Ca^{2+} during the MD trajectory at 50 ns, which shows that both glutamate residues, E31 and E67, kept their bidentate coordination of the Ca^{2+} ion (**Fig. S7** and **S16**). It is worth nothing that in Clb+Ca^{2+} E27 and E65 provide the bidentate coordination for Ca^{2+} in the pseudo EF-hand I and the canonical EF-hand II, respectively, without conformational change in this EF-hand domain. In addition, although we have exchanged the whole pseudo EF-hand I in Clb with the canonical EF-hand I from N-Cam, the new hybrid ClbEF1 domain did not change conformation in the presence of Ca^{2+} and the Ca^{2+} binding affinity was similar to that of Clb [36]. However, in order for Clb+Ca^{2+} to adopt an open conformation, 15 residues were mutated in this EF-hand domain by their counterpart from calmodulin, which are not involved in Ca^{2+} coordination [74].

Our findings suggests that conformational change in Ca^{2+} sensor EF-hand domains do not rely exclusively on the Ca^{2+} binding alone as widely accepted [4-6, 25-30], but rather solvation energetics and the molecular composition at the local environment of key residues such as those at position 41 and 75 in N-Cam, play an important role in the conformational change of these domains. Indeed, this is largely corroborated by the fact that our variant L39F-QLKI+Ca^{2+} binds Ca^{2+} with largely higher affinity than QLKI+Ca^{2+}, slightly higher than N-CamY, and yet maintains its closed conformation in solution unchanged, as well as our MD simulation showing that N-CamY+Ca^{2+} can populate a closed conformation during the trajectory and without losing the bidentate coordination of Ca^{2+} ions by E31 and E67 (**Fig. S16**). Interestingly, since N-CamY+Ca^{2+} fluctuate

between open and closed conformations in our MD simulation trajectory, as also previously reported [58], suggests that while the solvation energetics are favorable for the opening of this domain, it will populate the full open structure only in the presence of its protein target, as observed in this work with QLKI+Ca^{2+} in the presence of PEG 400 or alcohols. However, reported open X-ray structures of N-CamY+Ca^{2+} exhibit substantial crystal contacts including the hydrophobic surface, necessary for binding to protein targets [75], suggesting that crystal packing may stabilize these fully open structures, as previously suggested [58]. In addition, our suggestion is supported by the conformational change of C-Cam that occurs when binding to several protein targets in the absence of Ca^{2+} [56, 63-65]. However, it is worth noting that this opening of C-Cam is partial which suggests that although Ca^{2+} is not necessary for the conformational change in this EF-hand domain, Ca^{2+} binding rather promotes the domain full opening. In fact, this is well emphasized in the conformational opening of QLKI+Ca^{2+} by the presence of PEG 400 or alcohols, where the Ca^{2+} was necessary for this domain to fully open, while in the absence of Ca^{2+} QLKI remained closed.

5. Conclusion

Although the crystal structure of QLKI+Ca^{2+} revealed an open conformation that contradicts our previous finding of its closed conformation in solution, it provides us with an opportunity to finally supply experimental evidence of the intermediate conformational states of N-CamY+Ca^{2+} prior to its final open conformational state. Indeed, these intermediate conformational states include also the early stages mimic of the interactions of N-CamY+Ca^{2+} with its protein targets as shown in the progressive opening of QLKI+Ca^{2+} in solution when increasing the amount of either PEG400 or alcohols.

Our MD simulations clearly showed that QLKI+Ca^{2+} populates the closed form in solution, as we reported previously for QLKI+Ca^{2+} in solution [35], N-CamY+Ca^{2+} can populate the closed form in solution as previously reported [58], and suggested that the flexibility of the Ca^{2+} loops in the apo-form of these EF-hand domains may explain the differences of their Ca^{2+} affinity, as reported here for QLKI. Importantly, our MD simulations and structural energy minimizations provide structural evidence that QLKI+Ca^{2+} can have its Ca^{2+} ions bound by E31 and E67 via their bidentate coordination and maintains its closed conformation in solution.

Together our experimental and computational data show that the conformational change in Ca^{2+} sensor EF-hand domains depends on solvation enegetics, Ca^{2+} depleted state conformational dynamics, Ca^{2+} binding to promote the full open form, and the molecular composition, which reflect the presence of protein target of these domains, nearby residues at the C-terminal of H2, including part of the loop between H2 and H3, and the C-terminal of H4, and in particular at the corresponding positions of 41 and 75 in N-Cam.

Acknowledgments

We thank the beamline staff at the European Synchrotron Radiation Facility (Grenoble, France) for their help. We thank the Department of Pathology at University of Cambridge (Cambridge, UK) and the Department of Structural and Molecular Biology at University College London (London, UK) for their support.

References

[1] R.R. Biekofsky, J. Feeney, Cooperative cyclic interactions involved in metal binding to pairs of sites in EF-hand proteins, FEBS Lett, 439 (1998) 101-106.
[2] M.R. Nelson, E. Thulin, P.A. Fagan, S. Forsen, W.J. Chazin, The EF-hand domain: a globally cooperative structural unit, Protein Sci, 11 (2002) 198-205.
[3] R.H. Kretsinger, C.E. Nockolds, Carp muscle calcium-binding protein. II. Structure determination and general description, J Biol Chem, 248 (1973) 3313-3326.
[4] J.L. Gifford, M.P. Walsh, H.J. Vogel, Structures and metal-ion-binding properties of the Ca2+-binding helix-loop-helix EF-hand motifs, Biochem J, 405 (2007) 199-221.
[5] M.R. Nelson, W.J. Chazin, Structures of EF-hand Ca(2+)-binding proteins: diversity in the organization, packing and response to Ca2+ binding, Biometals, 11 (1998) 297-318.
[6] K.L. Yap, J.B. Ames, M.B. Swindells, M. Ikura, Diversity of conformational states and changes within the EF-hand protein superfamily, Proteins, 37 (1999) 499-507.
[7] K. Denessiouk, S. Permyakov, A. Denesyuk, E. Permyakov, M.S. Johnson, Two structural motifs within canonical EF-hand calcium-binding domains identify five different classes of calcium buffers and sensors, PLoS One, 9 (2014) e109287.
[8] A. Astegno, V. La Verde, V. Marino, D. Dell'Orco, P. Dominici, Biochemical and biophysical characterization of a plant calmodulin: Role of the N- and C-lobes in calcium

binding, conformational change, and target interaction, Biochim Biophys Acta, 1864 (2016) 297-307.

[9] J.L. Gifford, M. Jamshidiha, J. Mo, H. Ishida, H.J. Vogel, Comparing the calcium binding abilities of two soybean calmodulins: towards understanding the divergent nature of plant calmodulins, Plant Cell, 25 (2013) 4512-4524.

[10] H. Kawasaki, R.H. Kretsinger, Structural differences among subfamilies of EF-hand proteins--a view from the pseudo two-fold symmetry axis, Proteins, 82 (2014) 2915-2924.

[11] H. Kawasaki, R.H. Kretsinger, Analysis of the movements of helices in EF-hands, Proteins, 80 (2012) 2592-2600.

[12] S.P. Harborne, J.J. Ruprecht, E.R. Kunji, Calcium-induced conformational changes in the regulatory domain of the human mitochondrial ATP-Mg/Pi carrier, Biochim Biophys Acta, 1847 (2015) 1245-1253.

[13] M.T. Henzl, A.G. Sirianni, W.G. Wycoff, A. Tan, J.J. Tanner, Solution structures of polcalcin Phl p 7 in three ligation states: Apo-, hemi-Mg2+-bound, and fully Ca2+-bound, Proteins, 81 (2013) 300-315.

[14] A.M. Kilpatrick, J.E. Honts, H.M. Sleister, C.A. Fowler, Solution NMR structures of the C-domain of Tetrahymena cytoskeletal protein Tcb2 reveal distinct calcium-induced structural rearrangements, Proteins, 84 (2016) 1748-1756.

[15] M.X. Li, P.M. Hwang, Structure and function of cardiac troponin C (TNNC1): Implications for heart failure, cardiomyopathies, and troponin modulating drugs, Gene, 571 (2015) 153-166.

[16] R.K. Makiyama, C.A. Fernandes, T.R. Dreyer, B.S. Moda, F.F. Matioli, M.R. Fontes, I.G. Maia, Structural and thermodynamic studies of the tobacco calmodulin-like rgs-CaM protein, Int J Biol Macromol, 92 (2016) 1288-1297.

[17] T. Miyakawa, H. Shinomiya, F. Yumoto, Y. Miyauchi, H. Tanaka, T. Ojima, Y.S. Kato, M. Tanokura, Different Ca(2)(+)-sensitivities between the EF-hands of T- and L-plastins, Biochem Biophys Res Commun, 429 (2012) 137-141.

[18] N. Suzuki, S. Ban, E. Itoh, S. Chen, F.L. Imai, Y. Sawano, T. Miyakawa, M. Tanokura, N. Yonezawa, Calcium-dependent structural changes in human reticulocalbin-1, J Biochem, 155 (2014) 281-293.

[19] R.D. Burgoyne, D.W. O'Callaghan, B. Hasdemir, L.P. Haynes, A.V. Tepikin, Neuronal Ca2+-sensor proteins: multitalented regulators of neuronal function, Trends Neurosci, 27 (2004) 203-209.

[20] F. Haeseleer, Y. Imanishi, I. Sokal, S. Filipek, K. Palczewski, Calcium-binding proteins: intracellular sensors from the calmodulin superfamily, Biochem Biophys Res Commun, 290 (2002) 615-623.

[21] B. Honore, The rapidly expanding CREC protein family: members, localization, function, and role in disease, Bioessays, 31 (2009) 262-277.

[22] M. Ikura, J.B. Ames, Genetic polymorphism and protein conformational plasticity in the calmodulin superfamily: two ways to promote multifunctionality, Proc Natl Acad Sci U S A, 103 (2006) 1159-1164.

[23] D.J. O'Connell, M.C. Bauer, J. O'Brien, W.M. Johnson, C.A. Divizio, S.L. O'Kane, T. Berggard, A. Merino, K.S. Akerfeldt, S. Linse, D.J. Cahill, Integrated protein array screening and high throughput validation of 70 novel neural calmodulin-binding proteins, Mol Cell Proteomics, 9 (2010) 1118-1132.

[24] H. Tidow, P. Nissen, Structural diversity of calmodulin binding to its target sites, FEBS J, 280 (2013) 5551-5565.

[25] Z. Grabarek, Structural basis for diversity of the EF-hand calcium-binding proteins, J Mol Biol, 359 (2006) 509-525.

[26] S. Bhattacharya, C.G. Bunick, W.J. Chazin, Target selectivity in EF-hand calcium binding proteins, Biochim Biophys Acta, 1742 (2004) 69-79.

[27] W.J. Chazin, Relating form and function of EF-hand calcium binding proteins, Acc Chem Res, 44 (2011) 171-179.

[28] Z. Grabarek, Insights into modulation of calcium signaling by magnesium in calmodulin, troponin C and related EF-hand proteins, Biochim Biophys Acta, 1813 (2011) 913-921.

[29] S.Y. Lau, E. Procko, R. Gaudet, Distinct properties of Ca2+-calmodulin binding to N- and C-terminal regulatory regions of the TRPV1 channel, J Gen Physiol, 140 (2012) 541-555.

[30] J.L. Fallon, M.R. Baker, L. Xiong, R.E. Loy, G. Yang, R.T. Dirksen, S.L. Hamilton, F.A. Quiocho, Crystal structure of dimeric cardiac L-type calcium channel regulatory domains bridged by Ca2+* calmodulins, Proc Natl Acad Sci U S A, 106 (2009) 5135-5140.

[31] D. Shukla, A. Peck, V.S. Pande, Conformational heterogeneity of the calmodulin binding interface, Nat Commun, 7 (2016) 10910.

[32] J.B. Ames, S. Lim, Molecular structure and target recognition of neuronal calcium sensor proteins, Biochim Biophys Acta, 1820 (2012) 1205-1213.

[33] C.B. Marshall, T. Nishikawa, M. Osawa, P.B. Stathopulos, M. Ikura, Calmodulin and STIM proteins: Two major calcium sensors in the cytoplasm and endoplasmic reticulum, Biochem Biophys Res Commun, 460 (2015) 5-21.

[34] M. Shen, N. Zhang, S. Zheng, W.B. Zhang, H.M. Zhang, Z. Lu, Q.P. Su, Y. Sun, K. Ye, X.D. Li, Calmodulin in complex with the first IQ motif of myosin-5a functions as an intact calcium sensor, Proc Natl Acad Sci U S A, 113 (2016) E5812-E5820.

[35] A. Ababou, J.R. Desjarlais, Solvation energetics and conformational change in EF-hand proteins, Protein Sci, 10 (2001) 301-312.

[36] A. Ababou, R.A. Shenvi, J.R. Desjarlais, Long-range effects on calcium binding and conformational change in the N-domain of calmodulin, Biochemistry, 40 (2001) 12719-12726.

[37] A. Ababou, M. Zaleska, Electrostatics effects on Ca(2+) binding and conformational changes in EF-hand domains: Functional implications for EF-hand proteins, Arch Biochem Biophys, 587 (2015) 61-69.

[38] T.G. Battye, L. Kontogiannis, O. Johnson, H.R. Powell, A.G. Leslie, iMOSFLM: a new graphical interface for diffraction-image processing with MOSFLM, Acta Crystallogr D Biol Crystallogr, 67 (2011) 271-281.

[39] M.D. Winn, C.C. Ballard, K.D. Cowtan, E.J. Dodson, P. Emsley, P.R. Evans, R.M. Keegan, E.B. Krissinel, A.G. Leslie, A. McCoy, S.J. McNicholas, G.N. Murshudov, N.S. Pannu, E.A. Potterton, H.R. Powell, R.J. Read, A. Vagin, K.S. Wilson, Overview of the CCP4 suite and current developments, Acta Crystallogr D Biol Crystallogr, 67 (2011) 235-242.

[40] A.J. McCoy, R.W. Grosse-Kunstleve, P.D. Adams, M.D. Winn, L.C. Storoni, R.J. Read, Phaser crystallographic software, J Appl Crystallogr, 40 (2007) 658-674.

[41] A. Vagin, A. Teplyakov, Molecular replacement with MOLREP, Acta Crystallogr D Biol Crystallogr, 66 (2010) 22-25.

[42] F. DiMaio, N. Echols, J.J. Headd, T.C. Terwilliger, P.D. Adams, D. Baker, Improved low-resolution crystallographic refinement with Phenix and Rosetta, Nat Methods, 10 (2013) 1102-1104.

[43] P.D. Adams, P.V. Afonine, G. Bunkoczi, V.B. Chen, I.W. Davis, N. Echols, J.J. Headd, L.W. Hung, G.J. Kapral, R.W. Grosse-Kunstleve, A.J. McCoy, N.W. Moriarty, R. Oeffner, R.J. Read, D.C. Richardson, J.S. Richardson, T.C. Terwilliger, P.H. Zwart, PHENIX: a comprehensive Python-based system for macromolecular structure solution, Acta Crystallogr D Biol Crystallogr, 66 (2010) 213-221.

[44] P. Emsley, B. Lohkamp, W.G. Scott, K. Cowtan, Features and development of Coot, Acta Crystallogr D Biol Crystallogr, 66 (2010) 486-501.

[45] D.A. Case, V. Babin, J.T. Berryman, R.M. Betz, Q. Cai, D.S. Cerutti, T.E. Cheatham, III,, T.A. Darden, R.E. Duke, H. Gohlke, A.W. Goetz, S. Gusarov, N. Homeyer, P. Janowski, J. Kaus, I. Kolossváry, A. Kovalenko, T.S. Lee, S. LeGrand, T. Luchko, R. Luo, B. Madej, K.M. Merz, F. Paesani, D.R. Roe, A. Roitberg, C. Sagui, R. Salomon-Ferrer, G. Seabra, C.L. Simmerling, W. Smith, J. Swails, R.C. Walker, J. Wang, R.M. Wolf, X. Wu, P.A. Kollman, AMBER 14, University of California, San Francisco, (2014).

[46] T.E. Cheatham, 3rd, P. Cieplak, P.A. Kollman, A modified version of the Cornell et al. force field with improved sugar pucker phases and helical repeat, J Biomol Struct Dyn, 16 (1999) 845-862.

[47] W.L. Jorgensen, J. Chandrasekhar, J.D. Madura, M.L. Klein, Comparison of simple potential functions for simulating liquid water, J Chem Phys, 79 (1983) 926–935.

[48] J. Ryckaert, G. Ciccotti, H. Berendsen, Numerical integration of the Cartesian equations of motion for a system with constraints: molecular dynamics of n-alkanes, J Comput Phys, 23 (1977) 327–341.

[49] T.A. Darden, D. York, L. Pedersen, Particle Mesh Ewald: an N log(N) method for Ewald sums in large systems, J Chem Phys, 98 (1993) 10089-.

[50] J. Wang, W. Wang, P.A. Kollman, D.A. Case, Automatic atom type and bond type perception in molecular mechanical calculations, J Mol Graph Model, 25 (2006) 247-260.

[51] J. Wang, R.M. Wolf, J.W. Caldwell, P.A. Kollman, D.A. Case, Development and testing of a general amber force field, J Comput Chem, 25 (2004) 1157-1174.

[52] W. Humphrey, A. Dalke, K. Schulten, VMD: visual molecular dynamics, J Mol Graph, 14 (1996) 33-38.

[53] R. Chattopadhyaya, W.E. Meador, A.R. Means, F.A. Quiocho, Calmodulin structure refined at 1.7 A resolution, J Mol Biol, 228 (1992) 1177-1192.

[54] R.M. Fancy, L. Wang, T. Napier, J. Lin, G. Jing, A.L. Lucius, J.M. McDonald, T. Zhou, Y. Song, Characterization of calmodulin-Fas death domain interaction: an integrated experimental and computational study, Biochemistry, 53 (2014) 2680-2688.

[55] Z. Song, X. Zheng, B. Yang, Conformational stability of CopC and roles of residues Tyr79 and Trp83, Protein Sci, 22 (2013) 1519-1530.

[56] Q. Lu, J. Li, F. Ye, M. Zhang, Structure of myosin-1c tail bound to calmodulin provides insights into calcium-mediated conformational coupling, Nat Struct Mol Biol, 22 (2015) 81-88.

[57] C. Wang, B.C. Chung, H. Yan, H.G. Wang, S.Y. Lee, G.S. Pitt, Structural analyses of Ca(2)(+)/CaM interaction with NaV channel C-termini reveal mechanisms of calcium-dependent regulation, Nat Commun, 5 (2014) 4896.

[58] D. Vigil, S.C. Gallagher, J. Trewhella, A.E. Garcia, Functional dynamics of the hydrophobic cleft in the N-domain of calmodulin, Biophys J, 80 (2001) 2082-2092.

[59] J. Kordel, D.A. Pearlman, W.J. Chazin, Protein solution structure calculations in solution: solvated molecular dynamics refinement of calbindin D9k, J Biomol NMR, 10 (1997) 231-243.

[60] L.A. Svensson, E. Thulin, S. Forsen, Proline cis-trans isomers in calbindin D9k observed by X-ray crystallography, J Mol Biol, 223 (1992) 601-606.

[61] A. Villarroel, M. Taglialatela, G. Bernardo-Seisdedos, A. Alaimo, J. Agirre, A. Alberdi, C. Gomis-Perez, M.V. Soldovieri, P. Ambrosino, C. Malo, P. Areso, The ever changing moods of calmodulin: how structural plasticity entails transductional adaptability, J Mol Biol, 426 (2014) 2717-2735.

[62] A.P. Yamniuk, H.J. Vogel, Calmodulin's flexibility allows for promiscuity in its interactions with target proteins and peptides, Mol Biotechnol, 27 (2004) 33-57.

[63] A. Houdusse, J.F. Gaucher, E. Krementsova, S. Mui, K.M. Trybus, C. Cohen, Crystal structure of apo-calmodulin bound to the first two IQ motifs of myosin V reveals essential recognition features, Proc Natl Acad Sci U S A, 103 (2006) 19326-19331.

[64] V. Kumar, V.P. Chichili, L. Zhong, X. Tang, A. Velazquez-Campoy, F.S. Sheu, J. Seetharaman, N.Z. Gerges, J. Sivaraman, Structural basis for the interaction of unstructured neuron specific substrates neuromodulin and neurogranin with Calmodulin, Sci Rep, 3 (2013) 1392.

[65] B. Chagot, W.J. Chazin, Solution NMR structure of Apo-calmodulin in complex with the IQ motif of human cardiac sodium channel NaV1.5, J Mol Biol, 406 (2011) 106-119.

[66] M.X. Li, S.M. Gagne, L. Spyracopoulos, C.P.A.M. Kloks, G. Audette, M. Chandra, R.J. Solaro, L.B. Smillie, B.D. Sykes, NMR studies of Ca2+ binding to the regulatory domains of cardiac and E41A skeletal muscle troponin C reveal the importance of site I to energetics of the induced structural changes, biochemistry, 36 (1997) 12519-12525.

[67] J. Evenas, S. Forsen, A. Malmendal, M. Akke, Backbone dynamics and energetics of a calmodulin domain mutant exchanging between closed and open conformations, J Mol Biol, 289 (1999) 603-617.

[68] A. Malmendal, J. Evenas, S. Forsen, M. Akke, Structural dynamics in the C-terminal domain of calmodulin at low calcium levels, J Mol Biol, 293 (1999) 883-899.

[69] Z. Grabarek, Structure of a trapped intermediate of calmodulin: calcium regulation of EF-hand proteins from a new perspective, J Mol Biol, 346 (2005) 1351-1366.

[70] B. Wimberly, E. Thulin, W.J. Chazin, Characterization of the N-terminal half-saturated state of calbindin D9k: NMR studies of the N56A mutant, Protein Sci, 4 (1995) 1045-1055.

[71] J. Evenas, A. Malmendal, E. Thulin, G. Carlstrom, S. Forsen, Ca2+ binding and conformational changes in a calmodulin domain, Biochemistry, 37 (1998) 13744-13754.

[72] S.M. Gagne, M.X. Li, B.D. Sykes, Mechanism of direct coupling between binding and induced structural change in regulatory calcium binding proteins, Biochemistry, 36 (1997) 4386-4392.

[73] J. Evenas, E. Thulin, A. Malmendal, S. Forsen, G. Carlstrom, NMR studies of the E140Q mutant of the carboxy-terminal domain of calmodulin reveal global conformational exchange in the Ca2+-saturated state, Biochemistry, 36 (1997) 3448-3457.

[74] C.G. Bunick, M.R. Nelson, S. Mangahas, M.J. Hunter, J.H. Sheehan, L.S. Mizoue, G.J. Bunick, W.J. Chazin, Designing sequence to control protein function in an EF-hand protein, J Am Chem Soc, 126 (2004) 5990-5998.

[75] S.E. O'Donnell, R.A. Newman, T.J. Witt, R. Hultman, J.R. Froehlig, A.P. Christensen, M.A. Shea, Thermodynamics and conformational change governing domain-domain interactions of calmodulin, Methods Enzymol, 466 (2009) 503-526.

Figure Legends:

Fig. 1. Crystal structure of QLKI+Ca^{2+} in open conformation. (A) Structural comparison between QLKI+Ca2+ (blue) and N-Cam+Ca2+ (green). (B) Structural comparison of the Ca2+ loops, I and II, between QLKI+Ca2+ (blue) and N-Cam+Ca2+ (green). (C) Close up view on the core and other hydrophobic residues from of the structural comparison between QLKI+Ca2+ (blue) and N-Cam+Ca2+ (green).

Fig. 2. Conformational changes of QLKI+Ca2+ and N-CamY+Ca2+ monitored by Near-UV CD spectroscopy. (A) Spectra of QLKI+Ca2+ and N-CamY+Ca2+ in buffer, and QLKI+Ca2+ in crystallization buffer. (B) Spectra of QLKI+Ca2+ and N-CamY+Ca2+ in buffer in the presence of 1 mM or 300 mM Ca2+. (C) Spectra change of QLKI+Ca2+ as a function of added amount of PEG400, in percentage, as represented at 277 nm.

.

Fig. 3. Presence of PEG400 molecule in the hydrophobic core of the crystal structure of QLKI+Ca2+. (A) Structure of QLKI+Ca2+ exhibiting the localization of PEG400 molecule along with residues L41 and I75. (B) 2Fo – Fc electron density map of PEG400 molecule contoured at 1.0 σ. (C) Fo – Fc omit map for PEG400 molecule contoured at 3.0 σ. (D) Close up view on PEG400 molecule and its immediate surrounding deep in the hydrophobic core of QLKI+Ca2+.

Fig. 4. Opening extent of QLKI+Ca2+ and N-CamY+Ca2+ domains in the presence of ethanol and isopropanol as monitored by Near-UV CD spectroscopy. (A) Molecular representation of Ethanol and Isopropanol. (B) Spectra change of QLKI+Ca2+ as a function of added amount of alcohols, in percentage, as represented at 277 nm. (C) Spectra change of N-CamY+Ca2+ as a function of added amount of alcohols, in percentage, as represented at 277 nm.

Fig. 5. Overall MD simulation trajectories comparison between N-CamY+Ca2+ (black), QLKI+Ca2+ (red) and Clb+Ca2+ (blue). (A) Principal component analysis as projected into PC1 and PC2 modes. (B) Proteins stability and structural variations as assessed by calculated RMSD's over the backbone atoms. (C) Proteins fluctuations as assessed by calculated RMSF's over the backbone atoms. (D) Mapping of the amino acids with RMSF's at regions (1), (2) and (3).

Fig. 6. MD simulations analysis for N-CamY+Ca2+ (black), QLKI+Ca2+ (red) and Clb+Ca2+ (blue). (A) Distance changes between residues at positions 41 and 75 in N-CamY+Ca2+ and QLKI+Ca2+, and residues L39 and I73 in Clb+Ca2+. (B) SASA changes for residue L32 in N-CamY+Ca2+ and QLKI+Ca2+, and residue L28 in Clb+Ca2+. (C) SASA changes for residue F68 in N-CamY+Ca2+ and QLKI+Ca2+, and residue F66 in Clb+Ca2+. (D) Interhelical angle changes between H1 and H2. (E) Interhelical angle changes between H1 and H3. (F) Interhelical angle changes between H3 and H4.

Fig. 7. MD simulation analysis of QLKI+Ca^{2+}-PEG400 (green) along with comparison to QLKI+Ca^{2+} (red). (A) Distance changes between residues L41 and I75. (B) Interhelical angle changes between H1 and H2. (C) Interhelical angle changes between H3 and H4. (D) Snapshots structures of QLKI+Ca^{2+}-PEG400 from the MD simulation trajectory at 0, 30, 70 and 100 ns, where PEG400 molecule is represented in sticks (carbon atoms in yellow and oxygen atoms in red). The α-helices are named as H1 to H4. (E) Structures overlay, at helices H3 and H4, between the snapshots, at 0, 30, 70 and 100 ns, and the closed form of N-Cam (PDB code 1CFD).

Fig. 8. Overlay of energy minimized structures of QCKC+Ca2+ (green) and modelled QLKI+Ca2+ (light blue) where Ca2+ loop I and II are able to coordinate Ca2+ by E31 and E67. (A) Ca2+ loops I and II, and (B) small β-sheet between I27 and I63.

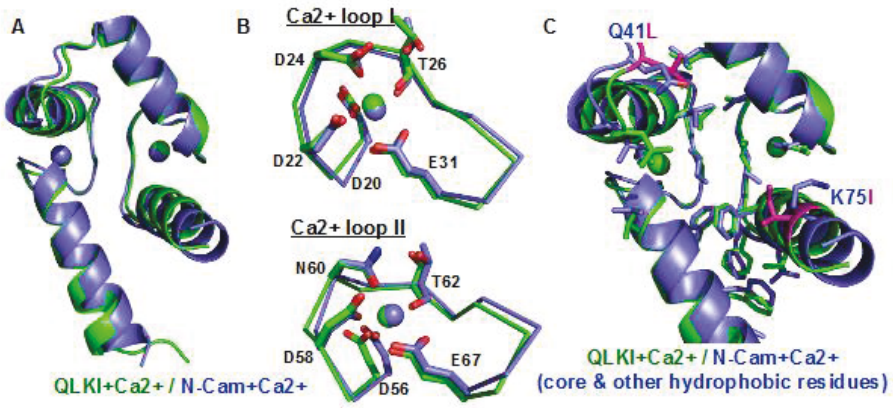

Fig. 1

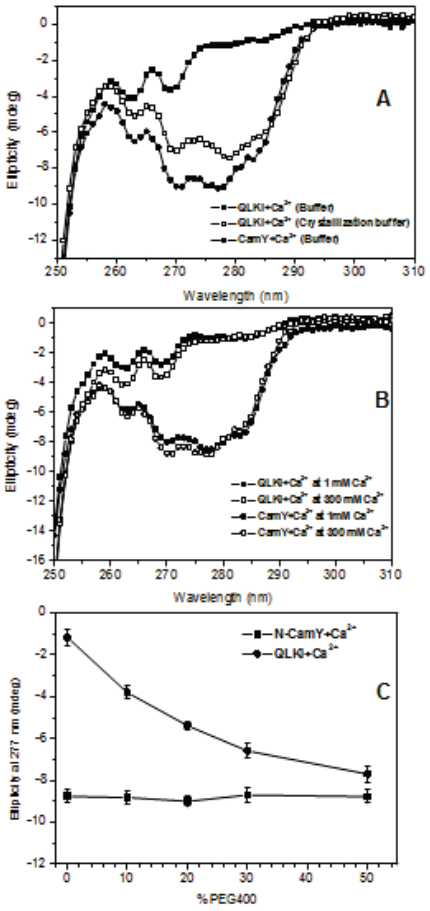

Fig. 2

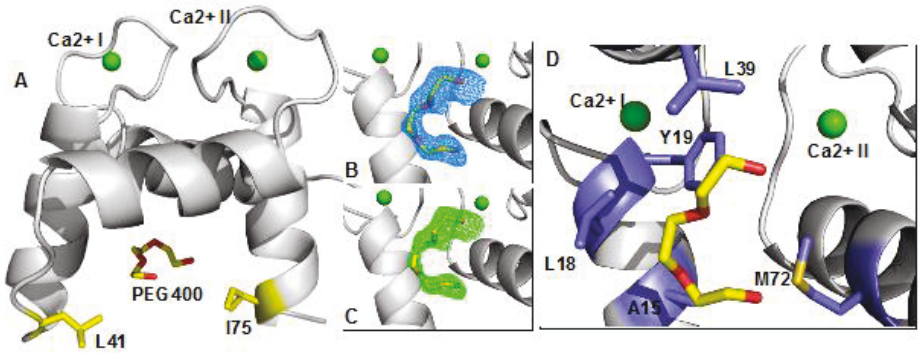

Fig. 3

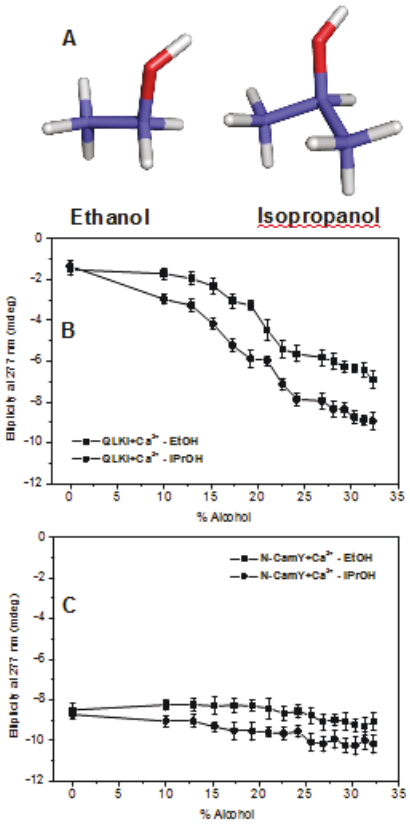

Fig. 4

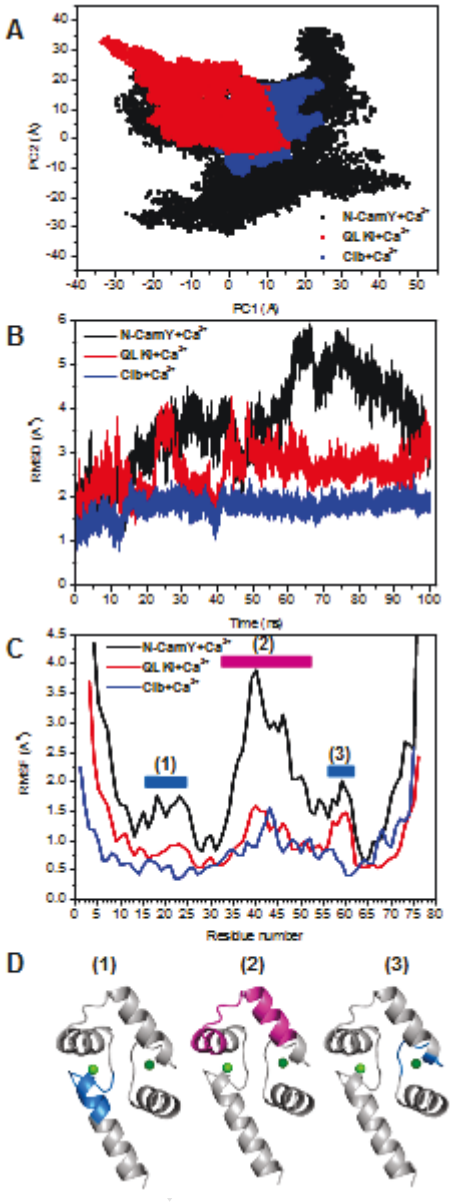

Fig. 5

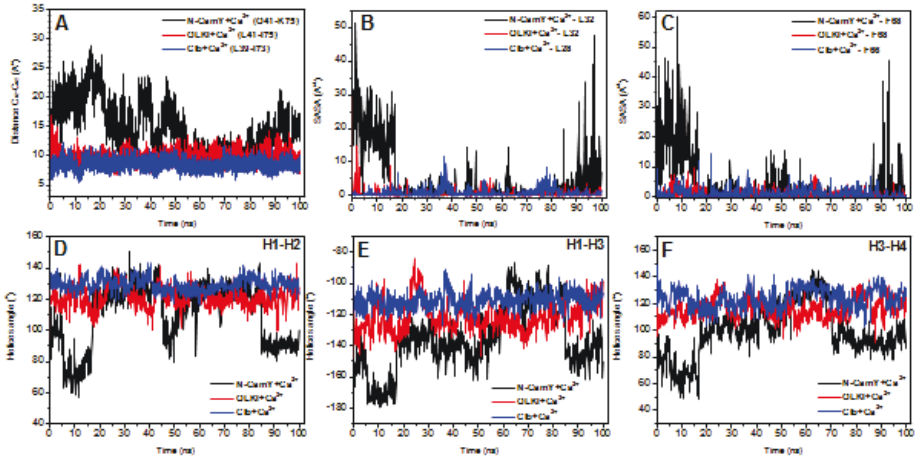

Fig. 6

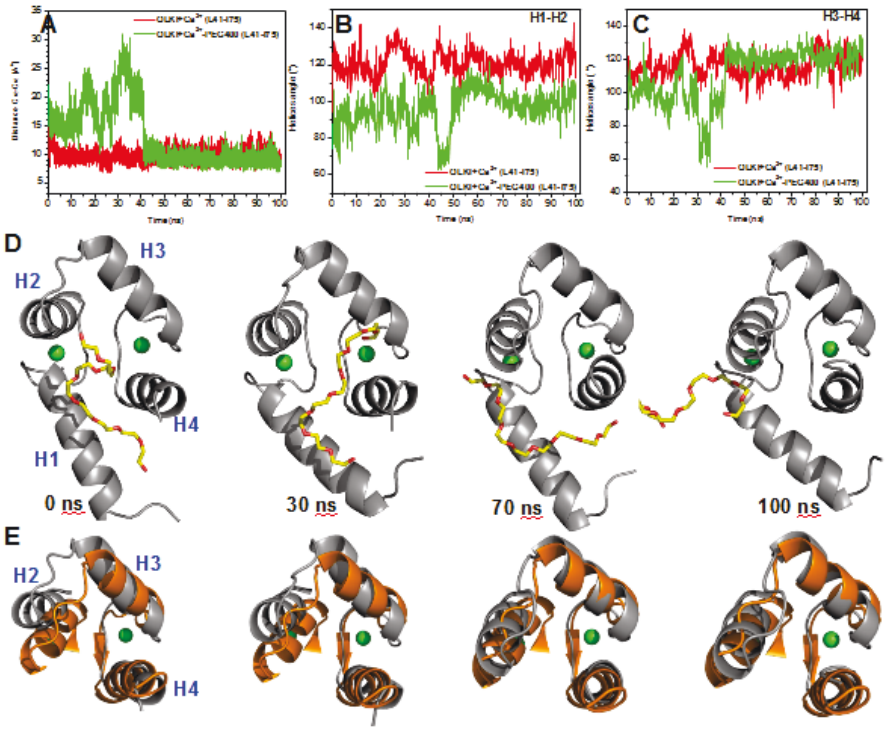

Fig. 7

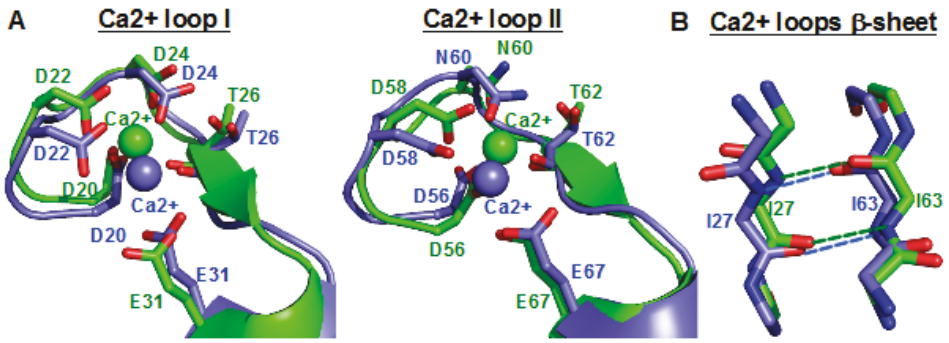

Fig. 8

Table 1
Data collection and refinement statistics.

Data collection	
Space group	P3221
Wavelength (Å)	1.0000
Unit cell:	
a, b, c (Å)	38.4, 38.4, 81.2
a , b, g (o)	90, 90, 120
Resolution range (Å)	
Overall (Å)	20.99 - 1.93
Outer shell (Å)	2.17 - 1.93
Completeness (%)	99.1 (97.5)
Unique reflections	5545
Rpim (%)	6.3 (30.1)
Redundancy	4.7 (3.6)
< I/s(I)>	6.8 (2.1)
Refinement	
Resolution range (Å)	20.99 – 1.93
Rwork (%)	22.9
Rfree (%)	26.4
Number of atoms	
Protein	583
Ligand/ion	12
Water	56
B-factor (Å2)	
Protein	29.0
Ligand/ion	32.7
Water	32.9
Model Geometry Quality	
RMSD bonds (Å)	0.012
RMSD angles (o)	1.31
Ramachandran analysis	
Fovoured (%)	99.0
Allowed (%)	1.0
Outliers (%)	0.0

Table 2 Comparison of interhelical angles between the four helices (H1, H2, H3, and H4) in N-Cam+Ca2+ (from 1CLL) and QLKI+Ca2+ (this work) domains' crystal structures.

	QLKI+Ca2+	N-Cam+Ca2+	Comparison
Helices	Angle	Angle	|Dang|[a]
H1-H2	95.71	87.67	8.04
H1-H3	-154.52	-160.55	6.03
H1-H4	101.72	106.60	4.87
H2-H3	105.66	111.63	5.97
H2-H4	-26.18	-40.99	14.81
H3-H4	92.06	87.75	4.31

[a]Absolute value of the angle difference

Graphical abstract

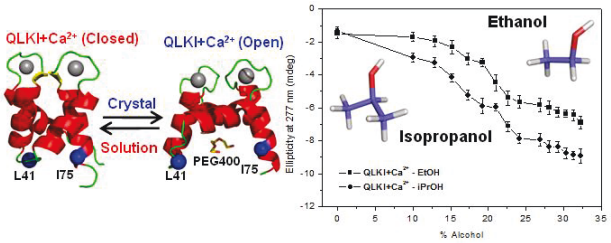

Highlights

- Crystal structure of QLKI+Ca^{2+} revealed an open conformation that contradicts its closed conformation in solution
- Addition of PEG400 or alcohols induces progressive conformational change of QLKI+Ca^{2+} in solution.
- Conformational change of QLKI+Ca^{2+} in solution provides experimental evidence on the intermediate conformations of N-Cam+Ca^{2+}
- Molecular dynamics of Ca^{2+} loops in QLKI may hold the answer to this domain low Ca^{2+} affinity compared to N-Cam